JOURNAL OF GUIDANCE, CONTROL, AND DYNAMICS
Vol. 28, No. 4, July–August 2005

Estimation of Postlaunch Angular Motion for Kinetic Energy Projectiles

William C. Pickel*
University of Texas at Austin, Austin, Texas 78759

Aerodynamic jump is a contributor to projectile launch dispersion errors. To reduce aerodynamic jump with an active control device, a method of estimating the aerodynamic jump is needed to identify the active control that is required. A method is developed for estimating the angular motion of a kinetic energy projectile immediately following launch. The sensors required are two body-fixed accelerometers nominally mounted on the projectile longitudinal axis, the nominal sensing axes of which are orthogonal to the longitudinal axis and orthogonal to each other. This estimation method permits the use of a body-fixed control device to reduce aerodynamic jump.

Nomenclature

$\boldsymbol{a}_{Bi}$	=	body frame inertial accelerations at the accelerometers, $i = 1, 2$
$a_{di}, \hat{a}_{di}$	=	A/D accelerometer output signals and their estimates, $i = 1, 2$
a_{mi}	=	accelerations sensed by the accelerometers, $i = 1, 2$
a_{ni}	=	nominal accelerometer signal model, $i = 1, 2$
$\boldsymbol{a}_{ni}$	=	nominal accelerations expected at the accelerometers, $i = 1, 2$
$\boldsymbol{B}$	=	inertial to body transformation matrix
$b_{ai}, \hat{b}_{ai}$	=	accelerometer biases and their estimates, $i = 1, 2$
$\boldsymbol{C}$	=	inertial to despun body transformation matrix
$C_X, C_{Na}, C_{Nq}, C_{L0}, C_P$	=	drag, normal force, pitch damping force, spin moment, and spin damping aerodynamic coefficients
d	=	projectile diameter
d_{ai}	=	nominal distance of the accelerometers behind the projectile center of gravity, $i = 1, 2$
$\boldsymbol{d}_{a1}, \boldsymbol{d}_{a2}$	=	vectors from the projectile center of gravity to the two accelerometer locations on the projectile
$\boldsymbol{d}_{Na}, \boldsymbol{d}_{Nq}$	=	vectors from the projectile center of gravity to the normal force and pitch damping force centers of pressure
$\boldsymbol{f}_g, \boldsymbol{f}_X, \boldsymbol{f}_{Na}, \boldsymbol{f}_{Nq}$	=	gravity force plus aerodynamic drag, normal, and pitch damping forces
g	=	gravity acceleration magnitude
$h_{\phi i}, h_{\upsilon i}, h_{\zeta I}, h_{\xi i}$	=	Kalman filter linear error observation coefficients
I_x, I	=	projectile roll and pitch inertias
$k_{L0}, k_P, \hat{k}_p$	=	roll moment and damping coefficients and the estimate of the roll damping coefficient
$k_{N\alpha}, k_{Nq}, \hat{k}_{N\alpha}, \hat{k}_{Nq}$	=	body angle and angular rate aerodynamic coefficients and their estimates
k_ζ, k_ξ	=	navigation model precession and nutation rates
$\boldsymbol{m}$	=	projectile mass
n_{ai}	=	accelerometer measurement noise, $i = 1, 2$
n_{di}	=	accelerometer signal digitization noise, $i = 1, 2$
$\hat{p}$	=	simulation roll rate estimate
$q_p, q_\upsilon, q_\zeta, q_{k\xi}$	=	error model propagation plant noise for roll moment, oscillation amplitude, precession angle and nutation rate, respectively
$\boldsymbol{R}$	=	projectile model roll transformation matrix
S	=	projectile aerodynamic reference area
s_{ai}	=	accelerometer measurement scale factor errors, $i = 1, 2$
$\boldsymbol{u}_{ai}$	=	accelerometer sensing direction unit vectors, $i = 1, 2$
V	=	projectile relative speed in the despun body frame
$\boldsymbol{v}$	=	projectile velocity vector in the despun body frame, $[v_1, v_2, v_3]^T$
$\boldsymbol{w}$	=	wind velocity vector in the despun body frame, $[w_1, w_2, w_3]^T$
$\boldsymbol{x}$	=	projectile inertial position vector
α, β	=	vertical and horizontal angle of attack components
$\hat{\alpha}, \hat{\beta}, \delta\alpha, \delta\beta$	=	navigator equivalent estimates and estimation errors for the vertical and horizontal angle of attack components
Δt	=	Kalman filter propagation time step
δ_{ai}	=	accelerometer error measurements, $i = 1, 2$
δr_{ai}	=	deviation of the accelerometer difference observations from a linear combination of the Kalman filter error states, $i = 1, 2$
$\delta\varphi, \delta p, \delta k_{L0}, \delta\upsilon, \delta\zeta, \delta\xi, \delta k_\xi, \delta b_{a1}, \delta b_{a2}$	=	Kalman filter error model variables for roll, roll rate, roll moment oscillation amplitude, precession angle, nutation angle, nutation rate, and two accelerometer biases, respectively
η, ν	=	navigator model of the perceived projectile angle of attack components
$\hat{\eta}, \hat{\nu}$	=	navigator estimates of the perceived projectile angle of attack components
μ_{ai}	=	unit vectors in the nominal orthogonal accelerometer sensing directions, $i = 1, 2$
ρ	=	air density
τ	=	navigator model of the projectile pitch–yaw oscillation magnitude decay time constant
υ, ξ, ζ	=	navigator model of the projectile pitch–yaw oscillation magnitude nutation angle and precession angle

Received 18 December 2003; revision received 5 November 2004; accepted for publication 18 November 2004.

*Research Scientist, Institute for Advanced Technology, 3925 West Braker Lane, Suite 4000; bill_pickel@iat.utexas.edu.

ϕ	=	projectile roll angle
ϕ_{ai}	=	nominal roll angles of the sensing axes of the two accelerometers, $i = 1, 2$
ϕ_0, θ_0, ψ_0	=	initial projectile roll and pitch and heading Euler angles, respectively
$\varphi, \hat{\varphi}$	=	navigator model of the projectile roll angle and its estimate
$\boldsymbol{\omega}_B = [p, q, r]^T$	=	angular rate vector of the body coordinate frame relative to the inertial coordinate frame
$\boldsymbol{\omega}_C = [0, \omega_2, \omega_3]^T$	=	angular rate vector of the despun body coordinate frame relative to the inertial coordinate frame
$\boldsymbol{\omega}_R = [p, 0, 0]^T$	=	angular rate vector of the body coordinate frame relative to the despun body coordinate frame

Introduction

DISPERSION reduction methods for projectiles and rockets that employ only onboard sensors have been examined recently. Kinetic energy projectile aerodynamic jump cancellation, the cancellation of lateral center of gravity motion resulting from pitch and yaw angular rates at launch, was demonstrated by using a timed rocket motor ignition in Ref. 1. Unfortunately, the effect of a rocket motor misalignment on performance was not examined. Lateral pulse jets or thrusters were used for active damping for rockets.[2] In addition, lateral thrusters have been used for dispersion control of rockets by controlling the trajectory to follow a prescribed trajectory[3] and by controlling the trajectory to a prescribed impact point.[4] The last three methods for dispersion control assumed that the required rocket states were available with no errors.

Whereas a transfer alignment and an inertial measurement unit can be used to provide accurate navigation on a rocket, it is virtually impossible on a projectile undergoing huge launch accelerations. A methodology for improving such navigation performance by estimating sensor biases on projectiles with inertial measurement units is presented in Ref. 5, but the effect of launch accelerations on the integration of the inertial measurement unit outputs could not be identified.

If the pitch motion of the projectile can be estimated with the aid of inertial sensors after launch, lateral thrusters can be used to reduce the aerodynamic jump by damping the pitching motion, as was done for rockets in Ref. 2. With both the sensor and the control devices fixed to the body of the projectile, estimation of the pitching motion is only required relative to a nonrolling coordinate frame. Knowledge of the orientation of the gravity vector in this coordinate frame is not required because only deviations of the projectile from its trajectory without aerodynamic jump are observable. This requires the observability of the roll rate and either the pitch and yaw motion of the projectile or the lateral acceleration of the projectile resulting from the pitch and yaw motion.

Fin-stabilized kinetic energy projectiles usually have small Magnus forces and moments[6] because the body surface is small. For these types of projectiles, the pitching motion looks like oscillations on a slowly rotating line segment. When a priori knowledge of the characteristics of the body motion based on its aerodynamic properties is used, the pitch and yaw motion of a projectile can be estimated using two accelerometers. If the projectile has negligible Magnus, the roll rate can also be accurately estimated using only the two accelerometers. A methodology for this body motion estimation is described for such projectiles.

Model of the Projectile Dynamics

The trajectory motion of the projectile is modeled by a rigid-body, longitudinal-axis symmetric, six-degree-of-freedom simulation.[7,8] Three coordinate frames are employed in the simulation. The first coordinate frame is an Earth-fixed frame the origin of which is at ground level at the projectile location at the end of the muzzle. Its first axis is horizontal, and its positive direction is nominally downrange. Its second axis is horizontal, perpendicular to the first axis, and its positive direction points to the right when looking downrange. Its third axis is vertical, perpendicular to the other two axes, with its positive direction pointing down. Coriolis and centripetal accelerations[9] resulting from the motion around the Earth and the Earth's rotation are considered negligible, and this coordinate frame is treated as if it is an inertial frame.

The second coordinate frame has its origin at the center of gravity of the projectile, and it moves and rotates with the projectile's motion and rotation. Its first axis points in the direction of its longitudinal axis of symmetry. The other two axes are orthogonal to the first axis and to each other and form a right-handed coordinate system. The initial relationship between the two coordinate frames is determined by the Euler angle transformation of a vector from the inertial frame to the body frame:

$$\boldsymbol{B} = \begin{bmatrix} c\theta_0 c\psi_0 & c\theta_0 s\psi_0 & -s\theta_0 \\ s\theta_0 c\psi_0 s\phi_0 - s\psi_0 c\phi_0 & s\theta_0 s\psi_0 s\phi_0 + c\psi_0 c\phi_0 & c\theta_0 s\phi_0 \\ s\theta_0 c\psi_0 c\phi_0 + s\psi_0 s\phi_0 & s\theta_0 s\psi_0 c\phi_0 - c\psi_0 s\phi_0 & c\theta_0 c\phi_0 \end{bmatrix} \qquad t = 0 \tag{1}$$

where $c\zeta$ and $s\zeta$ denote $\cos\zeta$ and $\sin\zeta$ for the angle ζ, respectively. Subsequent coordinate transformations between the two coordinate frames are defined by the solution of the matrix differential equation

$$\boldsymbol{B}' = \{\boldsymbol{\omega}_B\}\boldsymbol{B}, \qquad t \geq 0 \tag{2}$$

where

$$\boldsymbol{\omega}_B = [p, q, r]^T$$

is the angular rate column vector,

$$\{\boldsymbol{\omega}_B\} = \begin{bmatrix} 0 & r & -q \\ -r & 0 & p \\ q & -p & 0 \end{bmatrix}$$

and the superscript T denotes the transpose of a matrix or vector.

Let $\boldsymbol{R}$ be the roll transformation defined by

$$\boldsymbol{R} = \begin{bmatrix} 1 & 0 & 0 \\ 0 & c\phi & s\phi \\ 0 & -s\phi & c\phi \end{bmatrix} \tag{3}$$

with the roll angle ϕ defined as a function of time by the differential equation

$$\phi' = p, \qquad t \geq 0 \tag{4}$$

with initial condition

$$\phi = \phi_0, \qquad t = 0$$

Then, a third right-handed coordinate frame is defined by the matrix transformation

$$\boldsymbol{C} = \boldsymbol{R}^T\boldsymbol{B} \tag{5}$$

from inertial vectors to vectors in the third nonrolling coordinate frame. Initially, the first axis of this coordinate frame is in the direction of the first axis of the body frame, whereas the second axis is horizontal, and the third axis lies in the vertical plane containing the first axis.

Let

$$\boldsymbol{\omega}_R = [p, 0, 0]^T$$

$$\boldsymbol{\omega}_C = \boldsymbol{R}^T\boldsymbol{\omega}_B - \boldsymbol{\omega}_R = [0, \omega_2, \omega_3]^T \tag{6}$$

Then, the derivative of $\boldsymbol{C}$ is given by

$$\boldsymbol{C}' = -\boldsymbol{R}^T\{\boldsymbol{\omega}_R\}\boldsymbol{B} + \boldsymbol{R}^T\{\boldsymbol{\omega}_B\}\boldsymbol{B} = -\{\boldsymbol{\omega}_R\}\boldsymbol{R}^T\boldsymbol{B} + \left\{\boldsymbol{R}^T\boldsymbol{\omega}_B\right\}\boldsymbol{R}^T\boldsymbol{B}$$

$$= \{\boldsymbol{\omega}_C\}\boldsymbol{C}, \qquad t \geq 0 \tag{7}$$

The simulation constructs the roll matrix $\boldsymbol{R}$ using Eq. (3) and integrates the differential equation (4) by using the fourth-order Runga–Kutta integrator used in all simulation integrations. The matrix $\boldsymbol{C}$ is constructed, using Eq. (2-40) of Ref. 9, from the integral of the quaternion differential equation (2-41) in that reference, with initial values

$$[-s(\theta_0/2)\, s(\psi_0/2),\, s(\theta_0/2)\, c(\psi_0/2),$$

$$c(\theta_0/2)\, s(\psi_0/2),\, c(\theta_0/2)\, c(\psi_0/2)]^T$$

This quaternion is normalized to a magnitude of one on each integration step.

The matrix $\boldsymbol{B}$ is constructed by

$$\boldsymbol{B} = \boldsymbol{RC}, \qquad t \geq 0 \tag{8}$$

The inertial location of the projectile's center of gravity has the initial position vector $\boldsymbol{x}$ at time $t = 0$ and velocity vector

$$\boldsymbol{x}' = \boldsymbol{C}^T \boldsymbol{v}, \qquad t = 0$$

The inertial acceleration of the projectile center of gravity satisfies the differential equation

$$\boldsymbol{x}'' = \left[\boldsymbol{f}_g + \boldsymbol{C}^T(\boldsymbol{f}_X + \boldsymbol{f}_{N\alpha} + \boldsymbol{f}_{Nq})\right]/m \tag{9}$$

where $\boldsymbol{f}_g$ is the gravity force vector

$$\boldsymbol{f}_g = [0, 0, mg]^T$$

and $\boldsymbol{f}_X$, $\boldsymbol{f}_{N\alpha}$, and $\boldsymbol{f}_{Nq}$ are aerodynamic force vectors. Let

$$\boldsymbol{v} = \boldsymbol{Cx}' = [v_1, v_2, v_3]^T$$

let the wind speed in the nonrolling coordinate frame defined by $\boldsymbol{C}$ be

$$\boldsymbol{w} = [w_1, w_2, w_3]^T$$

let

$$V = \left[(v_1 - w_1)^2 + (v_2 - w_2)^2 + (v_3 - w_3)^2\right]^{\frac{1}{2}}$$

and let

$$\tan\alpha = (w_3 - v_3)/(v_1 - w_1), \qquad \tan\beta = (w_2 - v_2)/(v_1 - w_1)$$

where the positive direction of these angles is taken in the opposite direction relative to the definition of these angles in Ref. 7, p. 114. Then, approximating the results in Ref. 8, Chapter 2, the component aerodynamic force vectors are modeled by

$$\boldsymbol{f}_X = -\left(\tfrac{1}{2}\right)\rho V^2 S C_X [1, 0, 0]^T$$

$$\boldsymbol{f}_{N\alpha} = k_{N\alpha}[0, \beta, \alpha]^T, \qquad \boldsymbol{f}_{Nq} = k_{Nq}[0, \omega_3, -\omega_2]^T$$

with

$$k_{N\alpha} = \left(\tfrac{1}{2}\right)\rho V^2 S C_{N\alpha}, \qquad k_{Nq} = \left(\tfrac{1}{2}\right)\rho V S d C_{Nq}$$

The transformation of the angular acceleration equations of Ref. 7, p. 144, the assumption of symmetry about the longitudinal axis, and the aerodynamic equations in Ref. 8, Chapter 2, yield the angular acceleration in the nonrolling frame

$$p' = (k_{L0} - k_P p)/I_x \tag{10}$$

where

$$k_{L0} = \left(\tfrac{1}{2}\right)\rho V^2 S d C_{L0}, \qquad k_P = -\left(\tfrac{1}{2}\right)\rho V S d^2 C_P$$

and the angular accelerations in the nonrolling frame

$$\boldsymbol{\omega}'_C = \left(I_x p[0, -\omega_3, \omega_2]^T - \{\boldsymbol{d}_{N\alpha}\} f_{N\alpha} - \{\boldsymbol{d}_{Nq}\} f_{Nq}\right)/I \tag{11}$$

that are used in the simulation.

Accelerometer Model

The model of the two accelerometers assumes that the accelerometer locations on the projectile are defined by the body coordinate frame vectors $\boldsymbol{d}_{a1}$ and $\boldsymbol{d}_{a2}$ from the projectile center of gravity. The unit vectors $\boldsymbol{u}_{a1}$ and $\boldsymbol{u}_{a2}$ define the direction of a positive acceleration measurement for each of the accelerometers. The inertial location of the accelerometers is given by the inertial vector

$$\boldsymbol{p}_{ai} = \boldsymbol{x} + \boldsymbol{B}^T \boldsymbol{d}_{ai}$$

for $i = 1, 2$. The second derivative of this equation provides the inertial acceleration of the accelerometers in the inertial coordinate frame

$$\boldsymbol{p}''_{ai} = \boldsymbol{x}'' + \boldsymbol{B}''^T \boldsymbol{d}_{ai} = x'' + \boldsymbol{B}^T \{\boldsymbol{\omega}_B\}^2 \boldsymbol{d}_{ai} - \boldsymbol{B}^T \{\boldsymbol{\omega}'_B\} \boldsymbol{d}_{ai}$$

The transformation of these inertial accelerations to the body frame provides the inertial acceleration of the accelerometers in the body coordinate frame

$$\boldsymbol{a}_{Bi} = \boldsymbol{Bx}'' + \{\boldsymbol{\omega}_B\}^2 \boldsymbol{d}_{ai} - \{\boldsymbol{\omega}'_B\} \boldsymbol{d}_{ai} \tag{12}$$

for $i = 1, 2$. The simulation uses Eq. (12) for the calculation of these accelerations along with the calculations

$$\boldsymbol{\omega}_B = \boldsymbol{R\omega}_C + \boldsymbol{\omega}_R, \qquad \boldsymbol{\omega}'_B = \{\boldsymbol{\omega}_R\}\boldsymbol{R\omega}_C + \boldsymbol{R\omega}'_C + \boldsymbol{\omega}'_R \tag{13}$$

Because the accelerometer cannot observe the force of gravity in the gravity force field, the acceleration measured by each accelerometer is the acceleration component in the direction of its sensing axes less gravity, and it is modified by any scale factor error, bias, and measurement noise

$$a_{mi} = (1 + s_{ai})\boldsymbol{u}_{ai}^T(\boldsymbol{a}_{Bi} - \boldsymbol{B}\boldsymbol{f}_g/m) + b_{ai} + n_{ai} \tag{14}$$

for $i = 1, 2$. Equation (14) is used to generate the acceleration measurements in the simulation. In the simulation, the accelerometer measurements in Eq. (14) are passed through a 12-bit A/D converter, producing the digitized accelerometer measurements

$$a_{di} = a_{mi} + n_{di} \tag{15}$$

Nominal Accelerometer Placement and Orientation

To provide the best observability of the body motion, the accelerometers are nominally placed on the longitudinal axis of the projectile at distances d_{ai}, $i = 1, 2$, from the center of gravity. For this placement, the accelerations sensed by the accelerometers can be expressed as

$$\boldsymbol{a}_{ni} = \boldsymbol{R}(\boldsymbol{f}_X + \boldsymbol{f}_{N\alpha} + \boldsymbol{f}_{Nq})/m + \boldsymbol{R}\left[-r^2 - q^2, \omega'_3, -\omega'_2\right]^T d_{ai}$$

by using Eqs. (6), (9), (12), and (13). The nominal accelerometer alignment vectors are perpendicular to the longitudinal axis and perpendicular to each other. Therefore, they can be expressed as

$$\mu_{ai} = [0, \cos\phi_{ai}, \sin\phi_{ai}]^T$$

with

$$\phi_{a2} = \phi_{a1} + \pi/2$$

Consequently, the accelerations nominally observed by the accelerometers can be expressed as

$$a_{ni} = \mu_{ai}^T \boldsymbol{a}_{ni} = \cos(\phi + \phi_{ai})(k_{N\alpha}\beta + k_{Nq}\omega_3 + d_{ai}\omega'_3)$$

$$+ \sin(\phi + \phi_{ai})(k_{N\alpha}\alpha - k_{Nq}\omega_2 - d_{ai}\omega'_2)$$

Now,

$$a_{ni} = \cos(\phi + \phi_{ai})(k_{N\alpha}\beta + k_{Nq}\beta' + d_{ai}\beta'') + \sin(\phi + \phi_{ai})(k_{N\alpha}\alpha$$

$$+ k_{Nq}\alpha' + d_{ai}\alpha'') + \cos(\phi + \phi_{ai})(k_{Nq}\gamma_3 + d_{ai}\gamma'_3)$$

$$+ \sin(\phi + \phi_{ai})(k_{Nq}\gamma_2 + d_{ai}\gamma'_2)$$

where γ_2 and γ_3 are the angular rates of the velocity vector:

$$\gamma_2 = -\omega_2 - \alpha', \qquad \gamma_3 = \omega_3 - \beta'$$

Therefore, the accelerometer measurements can be expressed as

$$a_{di} = c(\phi + \phi_{ai})(k_{N\alpha}\beta + k_{Nq}\beta' + d_{ai}\beta'') + s(\phi + \phi_{ai}) \times (k_{N\alpha}\alpha + k_{Nq}\alpha' + d_{ai}\alpha'') + b_{ai} + r_{ai} \tag{16}$$

where r_{ai} includes the effects of noise, scale factor errors, accelerometer misalignment and position errors, and modeling approximations.

Simplified Angle-of-Attack Motion Model

Let φ be any body roll angle. Then, φ satisfies

$$\varphi' = p \tag{17}$$

as in Eq. (4). Let

$$\eta = \cos(\phi - \varphi)\beta + \sin(\phi - \varphi)\alpha$$

$$\nu = -\sin(\phi - \varphi)\beta + \cos(\phi - \varphi)\alpha$$

Then, the accelerometer measurement can be expressed as

$$a_{di} = c(\varphi + \phi_{ai})(k_{N\alpha}\eta + k_{Nq}\eta' + d_{ai}\eta'') + s(\varphi + \phi_{ai}) \times (k_{N\alpha}\nu + k_{Nq}\nu' + d_{ai}\nu'') + b_{ai} + r_{ai} \tag{18}$$

Simulation outputs of angle-of-attack motion over several pitch cycles for this type of projectile show that the body motion of the projectile is approximately a slowly decaying oscillation along a line segment that is slowly rotating about the velocity vector. This allows the body motion model approximation

$$\eta = \upsilon \cos\xi \cos\zeta \tag{19}$$

$$\nu = \upsilon \cos\xi \sin\zeta \tag{20}$$

where the oscillation magnitude υ decays via

$$\upsilon' = -\upsilon/\tau \tag{21}$$

the precession angle ζ satisfies

$$\zeta' = k_\zeta \tag{22}$$

and the nutation angle satisfies

$$\xi' = k_\xi \tag{23}$$

Equations (19–23) provide the means for approximating η', η'', ν', and ν'' for use with Eq. (18). Under the assumption that τ, k_ζ, and k_ξ are essentially constant during the estimation processing time interval, differentiation of Eqs. (19) and (20) produces

$$\eta' = -\upsilon c\xi c\zeta/\tau - k_\xi \upsilon s\xi c\zeta - k_\zeta \upsilon c\xi s\zeta \tag{24}$$

$$\eta'' = \upsilon c\xi c\zeta\left(1/\tau^2 - k_\xi^2 - k_\zeta^2\right) - 2(k_\xi \upsilon s\xi c\zeta + k_\zeta \upsilon c\xi s\zeta)/\tau + 2k_\xi k_\zeta \upsilon s\xi s\zeta \tag{25}$$

$$\nu' = -\upsilon c\xi s\zeta/\tau - k_\xi \upsilon s\xi s\zeta + k_\zeta \upsilon c\xi c\zeta \tag{26}$$

$$\nu'' = \upsilon c\xi s\zeta\left(1/\tau^2 - k_\xi^2 - k_\zeta^2\right) + 2(k_\xi \upsilon s\xi s\zeta - k_\zeta \upsilon c\xi c\zeta)/\tau - 2k_\xi k_\zeta \upsilon s\xi c\zeta \tag{27}$$

Projectile Angular Motion Estimation

Equations (10), (17), and (19–23) provide models for maintaining estimates of the projectile's angular motion over time for navigation. Navigation estimates of φ, p, υ, ζ, and ξ are required, with η and ν calculated from them. Navigation estimates of k_{L0}, k_P, τ, k_ζ, and k_ξ can be derived from aerodynamic models and simulation outputs. Equation (18), along with Eqs. (24–27), provides a model for comparing the accelerometer measurement observations of the projectile's angular motion with the estimated angular motion. Because the accelerometer measurements can include significant biases, estimates of these biases are also required. Estimation of other parameters could be needed, as well. For example, if the accelerometers cannot be placed sufficiently close to the projectile longitudinal axis, or the projectile aerodynamic roll axis is not sufficiently aligned with the projectile longitudinal axis and the accelerometers can not be placed close to the projectile center of gravity, the accelerometers will also sense centripetal accelerations that vary in proportion to the square of the roll rate. In this case, these two centripetal accelerations would have to be included in the accelerometer model in Eq. (18) and their distance from the roll axis estimated. Estimates of the coefficients $k_{N\alpha}$ and k_{Nq} for the measurement model in Eq. (18) can be derived from aerodynamic models.

Correction for errors in estimates of these body motion model states and accelerometer biases can be accomplished by using Kalman filter and extended Kalman filter techniques (see Ref. 10, Chapter 4, and Ref. 11, Chapters 4–6). An extended Kalman filter was developed and implemented in the simulation to correct the navigation state estimates. Discrete equivalents of the propagation Eqs. (10) and (17–23) are used. The measurement model in Eq. (18) is used to correct the estimates of φ, p, k_{L0}, υ, ζ, ξ, k_ξ, b_{a1}, and b_{a2}. When $\delta\varphi(k)$, $\delta p(k)$, $\delta k_{L0}(k)$, $\delta\upsilon(k)$, $\delta\zeta(k)$, $\delta\xi(k)$, $\delta k_\xi(k)$, $\delta b_{a1}(k)$, and $\delta b_{a2}(k)$ denote errors in the estimates on the kth step, respectively, the error propagation equations used to develop the discrete propagation of the error covariance matrix are

$$\delta\varphi(k) = \delta\varphi(k-1) + \delta p(k-1)\Delta t + [\delta k_{L0}(k-1) - \hat{k}_P \delta p(k-1)]\Delta t^2/2$$

$$\delta p(k) = \delta p(k-1) + [\delta k_{L0}(k-1) - \hat{k}_P \delta p(k-1)]\Delta t$$

$$\delta k_{L0}(k) = \delta k_{L0}(k-1) + q_p(k-1)$$

$$\delta\upsilon(k) = e^{-\Delta t/\tau}\delta\upsilon(k-1) + q_\upsilon(k-1)$$

$$\delta\zeta(k) = \delta\zeta(k-1) + q_\zeta(k-1)$$

$$\delta\xi(k) = \delta\xi(k-1) + \delta k_\xi(k-1)\Delta t$$

$$\delta k_\xi(k) = \delta k_\xi(k-1) + q_{k\xi}(k-1)$$

$$\delta b_{a1}(k) = \delta b_{a1}(k-1), \qquad \delta b_{a2}(k) = \delta b_{a2}(k-1)$$

where Δt is the propagation time step, $\hat{k}_P$ is an estimate of k_P, and $q_p(k-1)$, $q_\upsilon(k-1)$, $q_\zeta(k-1)$ and $q_{k\xi}(k-1)$ are uncorrelated plant noise contributions to the errors resulting from model imperfections and approximations.

Estimates of the accelerometer measurements based on Eqs. (18) are formed from estimates of the model parameters by

$$\underline{\hat{a}}_{di}(k) = c(\hat{\varphi}_-(k) + \phi_{ai})(\hat{k}_{N\alpha}\hat{\eta}_-(k) + \hat{k}_{Nq}\underline{\hat{\eta}}(k)' + d_{ai}\underline{\hat{\eta}}(k)'') + s[\hat{\varphi}(k) + \phi_{ai})(\hat{k}_{N\alpha}\hat{\nu}(k) + \hat{k}_{N\alpha}\hat{\nu}(k)' + d_{ai}\hat{\nu}(k)''] + \hat{b}_{ai}$$

for $i = 1, 2$, where $\hat{\varphi}$, $\hat{k}_{N\alpha}$, $\hat{k}_{Nq}$, $\hat{\eta}$, $\hat{\nu}$, and $\hat{b}_{ai}$ are estimates of φ, $k_{N\alpha}$, k_{Nq}, η, ν, and b_{ai}, respectively. Error observations are formed by subtracting $\bar{a}_{di}(k)$ from $a_{di}(k)$, forming

$$\delta a_i(k) = a_{di}(k) - \bar{a}_{di}(k)$$

The error observations are then linearized with respect to the error variables for the construction of the Kalman filter corrections. This

yields an error model having the form

$$\delta a_i(k) = h_{\varphi i}(k)\delta\varphi(k) + h_{\upsilon i}(k)\delta\upsilon(k) + h_{\zeta i}(k)\delta\zeta(k) + h_{\xi i}(k)\delta_\xi(k) + \delta b_{ai}(k) + \delta r_{ai}(k)$$

where $h_{\varphi i}(k)$, $h_{\upsilon i}(k)$, $h_{\zeta i}(k)$, and $h_{\xi i}(k)$, the observation coefficients, are functions of the estimates, and where $\delta r_{ai}(k)$ is the sum of r_{ai} plus terms containing higher-order products of the error variables. The Kalman filter uses second-order filter methods (Ref. 11, pp. 191, 192) to account for the second-order error contributions to $\delta r_{ai}(k)$. No other correlations for these measurement error noise terms are assumed in the Kalman filter implementation.

Results

The simulated projectile is a 7.425-kg fin-stabilized projectile that is 0.7728 m long and has a center of gravity location 0.3864 m from the nose. The pitch and roll moments of inertia are 0.4071 and 0.0008518 kg · m^2, respectively. It exits the barrel at the time $t = 0$ at the vector $\boldsymbol{x} = [0, 0, -2]^T$ m with an initial speed of 1700 m/s pointed in the direction of the body longitudinal axis of symmetry. The initial Euler angles are $\psi_0 = 0$ deg, $\theta_0 = 0.495$ deg, and $\phi_0 = 0$ deg. The roll rate at time $t = 0$ is $p = 0$ deg/s, but the angular rates ω_2 and ω_3 can be nonzero. An initial nonlinear ramp of the air density to its nominal value after launch is included to represent the effect of gun gases on aerodynamics. This ramp was extended to 5 ms from launch to show the convergence of the roll rate estimation.

The simulation has nominal accelerometer locations of 0.7 and 0.72 m behind the nose on the longitudinal axis of symmetry. The simulated accelerometers have a measurement range between 800 and −800 m/s^2. This range is adequate to observe the measured accelerations for a projectile pitch oscillation with as much as a 6-deg amplitude in the presence of accelerometer bias, scale factor, location, sensing direction, and random measurement errors. For each accelerometer, the simulation randomly selects at initialization a bias, a scale factor error, a location error, and sensing axis direction errors from zero mean normal distributions having standard deviations of 80 m/s^2, 0.1%, 0.2 mm, and 0.2 deg, respectively. The standard deviation of the zero mean distribution of the random error contribution to each measurement is 0.8 m/s^2, which is approximately twice the resolution of the 12-bit A/D converter. A 5-ms delay in the use of the accelerometer measurements is included to account for the accelerometer settling time from the large accelerations at launch. A longer settling time for the accelerometers would merely delay the implementation of the estimation process.

In addition to the estimates $\hat{\varphi}$, $\hat{\eta}$, and $\hat{\upsilon}$, let $\hat{p}$ be the estimate of the roll rate p. Then

$$\delta p = p - \hat{p}$$

In addition, the effective estimates of α and β are

$$\hat{\beta} = \cos(\phi - \hat{\varphi})\hat{\eta} - \sin(\phi - \hat{\varphi})\hat{\upsilon}$$

$$\hat{\alpha} = \sin(\phi - \hat{\varphi})\hat{\eta} + \cos(\phi - \hat{\varphi})\hat{\upsilon}$$

The error in the estimates of α and β are

$$\delta\beta = \beta - \hat{\beta}, \qquad \delta\alpha = \alpha - \hat{\alpha}$$

The Kalman filter initial conditions are given in Table 1 with nondiagonal error covariance matrix entries equal to zero. Because there are no "true" simulation states for the model parameters υ, ζ, and ξ, the initial estimation errors in Table 1 are based on estimates after convergence of the Kalman filter. Also, convergence of the estimates of υ and ζ can also converge to $-\upsilon$ and $\zeta + \pi$. Moreover, the direction of the estimate of ζ will be rotated from the true oscillation direction by the difference $\phi - \hat{\varphi}$ after filter convergence. This difference initially is 1.047 rad, but changes because of the initial air density model. This air density model is also the primary reason for the large initial variance for δp in Table 1. The initial error $\delta\varphi$ is zero because φ can be any roll angle. The initial roll rate error is zero under the assumption that the projectile is not rolling initially.

Table 1 Initial errors

Error state	First example initial error	Initial error variance
$\delta\varphi$	0 rad	0.000001 rad^2
δp	0 rad/s	100 rad^2/s^2
δk_{L0}	4 rad/s^2	4 rad^2/s^4
$\delta\upsilon$	0.105 rad	0.0025 rad^2
$\delta\zeta$	0.922 rad	1 rad^2
$\delta\xi$	0.15 rad	0.04 rad^2
δk_ξ	−1.7 rad/s	1 rad^2/s^2
δb_{a1}	−178. m/s^2	6400 m^2/s^4
δb_{a2}	−7 m/s^2	6400 m^2/s^4

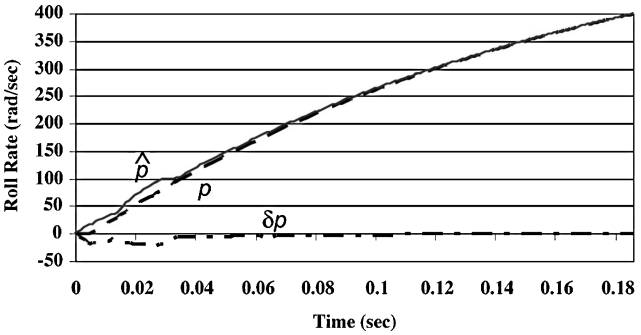

Fig. 1 First example: roll rate, estimate, and error.

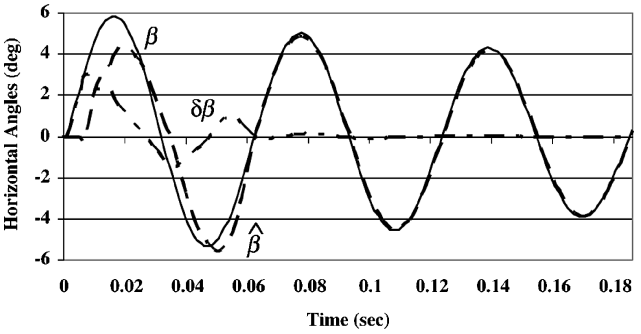

Fig. 2 First example: horizontal angle-of-attack component, estimate, and error.

The initial error listed for δk_{L0} is the error after the air density has reached its full magnitude. The Kalman filter estimator error measurement noise variance used for each accelerometer measurement, not including higher-order error state products, was 9 m^2/s^4. The nominal plant noise variances for q_p, q_υ, q_ζ, and $q_{k\xi}$ used in the Kalman filter were 0.004 rad^2/s^4, 0.0000025 rad^2, 0.000001 rad^2, and 0.001 rad^2/s^2, respectively.

In the first example, the simulation used launch angular rates of

$$\omega_2 = 0 \text{ rad/s}, \qquad \omega_3 = 10 \text{ rad/s}$$

at $t = 0$, which produce a peak oscillation of close to 6 deg in the horizontal direction with little vertical angular motion over the first three pitch cycles. The roll rate, roll rate estimate, and roll rate estimation error are shown in Fig. 1, where it can be seen that most of the roll rate estimation error is eliminated by 0.04 s, or approximately two-thirds of a pitch cycle. The horizontal and vertical components of angle of attack, their estimates, and their estimation errors are shown in Figs. 2 and 3. The horizontal estimation error $\delta\beta$ stays below 0.1 deg after approximately 1.5 pitch cycles, and the vertical estimation error stays below 0.1 deg after the first pitch cycle. Convergence of the two accelerometer bias estimates is shown in Figs. 4 and 5, where it can be seen that it takes approximately one pitch cycle to separate these constant contributions to the accelerometer measurements from the oscillatory contributions at the spin frequency and the pitch frequency. Note that the true angle-of-attack motion shown in Figs. 2 and 3 illustrate the approximate body motion model

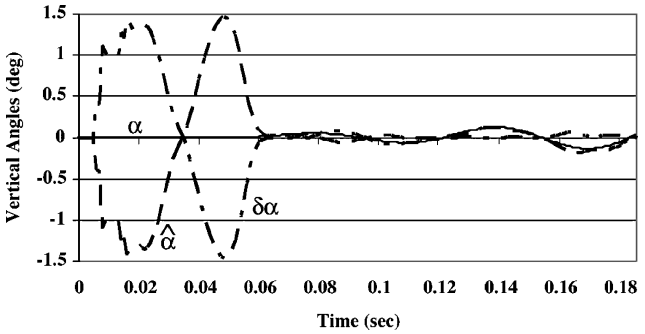

Fig. 3 First example: vertical angle-of-attack component, estimate, and error.

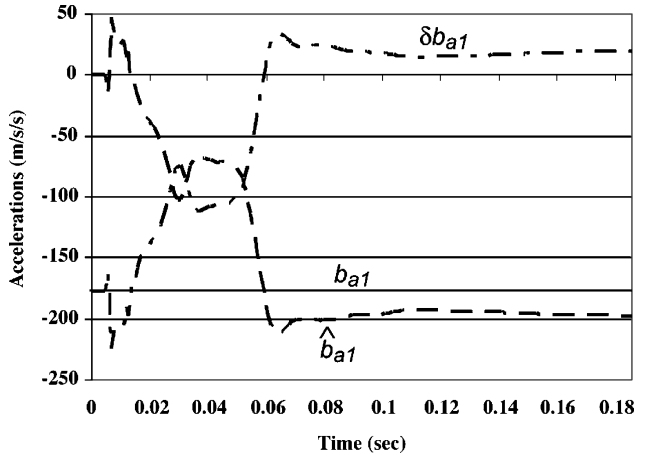

Fig. 4 First example: first accelerometer bias, bias estimate, and error.

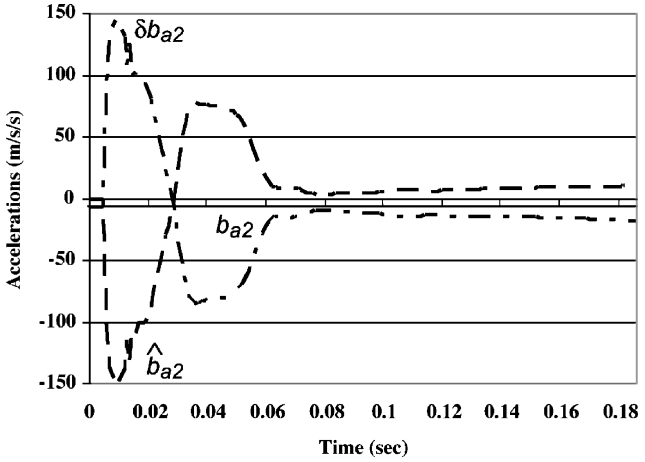

Fig. 5 First example: second accelerometer bias, bias estimate, and error.

presented in Eqs. (19–23) and can be used to estimate the parameters τ, k_ζ, and k_ξ.

In a second example, the simulation used launch angular rates of

$$\omega_2 = -1.414 \text{ rad/s} \qquad \omega_3 = -1.414 \text{ rad/s}$$

at $t = 0$. The magnitude of the peak oscillation is approximately one-fifth the magnitude of the peak oscillation in the first example. The peak accelerations sensed by the accelerometer are only slightly larger in magnitude than the magnitude of the acceleration bias standard deviations. Yet the estimation performance is similar to that in the first example as shown in Figs. 6–8. In Fig. 6, the roll rate, roll rate estimate, and roll rate estimation error are shown. The roll rate estimation error requires nearly a full pitch cycle to be effectively eliminated. In Figs. 7 and 8, the horizontal and vertical components of angle of attack, their estimates, and their estimation

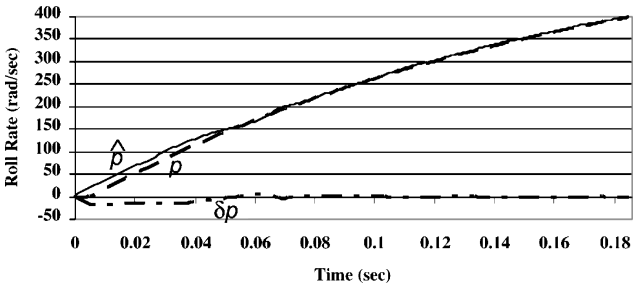

Fig. 6 Second example: roll rate, estimate, and error.

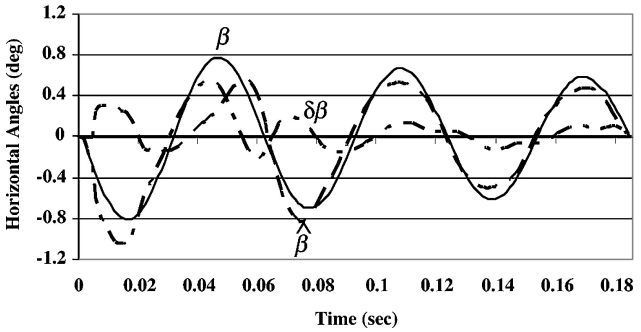

Fig. 7 Second example: horizontal angle-of-attack component, estimate, and error.

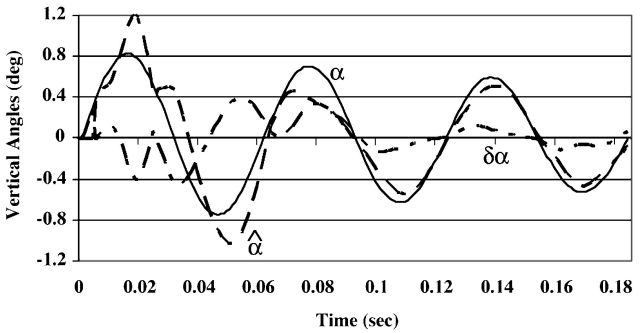

Fig. 8 Second example: vertical angle-of-attack component, estimate, and error.

errors are shown. The horizontal estimation error and the vertical estimation error both stay below 0.15 deg after 1.5 pitch cycles from launch.

Estimation accuracy can degrade with smaller initial angular rates because of lower acceleration amplitudes in the presence of the simulated accelerometer biases. The last example was rerun with angular rates having half the magnitude, with

$$\omega_2 = -0.707 \text{ rad/s}, \qquad \omega_3 = -0.707 \text{ rad/s}$$

at $t = 0$. All other initial conditions remained the same. The roll rate estimation error at the end of the third pitch cycle was approximately 8.6 rad/s. In the third pitch cycle, the peak estimation errors in both the horizontal and vertical directions were greater than 50% of the corresponding peak angle oscillations.

To examine the sensitivity to initial conditions, this simulation was rerun with no accelerometer biases, and it was rerun again with the accelerometer biases unchanged but with initial angular rates of

$$\omega_2 = 0.707 \text{ rad/s}, \qquad \omega_3 = -0.707 \text{ rad/s}$$

at $t = 0$. In both cases, performance of the estimation errors was better than the performance shown in Figs. 7 and 8, but with a slightly longer time for full convergence of the roll rate estimate shown in Fig. 6. Thus, estimation accuracy can be degraded for small launch angular rates in the presence of large accelerometer biases, depending on the relative values of the initial errors.

Conclusions

A method has been developed for estimating the angular motion of a kinetic energy projectile immediately following launch. The only sensors required are two body-fixed accelerometers nominally mounted on the projectile longitudinal axis, the nominal sensing axes of which are orthogonal to the longitudinal axis and orthogonal to each other. This estimation method provides the navigation capability to implement a guidance scheme with body-fixed control devices to reduce the aerodynamic jump of the projectile.

Acknowledgment

The research reported in this document was performed in connection with Contract DAAD17-01-D-0001 with the U.S. Army Research Laboratory. The views and conclusions contained in this document are those of the author and should not be interpreted as presenting the official policies or position, either expressed or implied, of the U.S. Army Research Laboratory or the U.S. Government unless so designated by other authorized documents. Citation of manufacturer's or trade names does not constitute an official endorsement or approval of the use thereof. The U.S. Government is authorized to reproduce and distribute reprints for Government purposes notwithstanding any copyright notation hereon.

References

[1]Grau, J., and Fiorellini, A., "Aerodynamic Jump Cancellation for a Kinetic Energy Projectile," AIAA Paper 94-0502, 1994.

[2]Harkins, T. E., and Brown, T. G., "Using Active Damping as a Precision-Enhancing Technology for 2.75-Inch Rockets," U.S. Army Research Lab., Rept. ARL-TR-1772, Aberdeen Proving Ground, MD, July 1999.

[3]Jitpraphai, T., and Costello, M., "Dispersion Reduction of a Direct Fire Rocket Using Later Pulse Jets," *Journal of Spacecraft and Rockets*, Vol. 38, No. 6, 2001, pp. 929–936.

[4]Burchett, B., and Costello, M., "Model Predictive Lateral Pulse Jet Control of an Atmospheric Rocket," *Journal of Guidance, Control, and Dynamics*, Vol. 25, No. 5, 2002, pp. 860–866.

[5]Burchett, B., and Costello, M., "Specialized Kalman Filtering for Guided Projectiles," AIAA Paper 2001-1120, 2001.

[6]Platou, A. S., "Magnus Characteristics of Finned and Nonfinned Projectiles," *AIAA Journal*, Vol. 3, No. 1, 1965, pp. 83–90.

[7]Etkin, B., *Dynamics of Atmospheric Flight*, Wiley, New York, 1972, pp. 104–195.

[8]McCoy, R. L., *Modern Exterior Ballistics*, Shiffer Military History, Atglen, PA, 1999, pp. 32–41.

[9]Farrell, J. L., *Integrated Aircraft Navigation*, Academic Press, New York, 1976, pp. 32–60.

[10]Luenberger, D. G., *Optimization By Vector Space Methods*, Wiley, New York, 1969, pp. 78–102.

[11]Gelb, A. (ed.), *Applied Optimal Estimation*, MIT Press, Cambridge, MA, 1974, pp. 102–228.